Multiwavelength ghost imaging

Deyang Duan,[1] Shaojiang Du,[2] and Yunjie Xia[1,*]

[1]*Shandong Provincial Key Laboratory of Laser Polarization and Information Technology, Research Institute of Laser, Qufu Normal University, Qufu 273165, China*

[2]*Department of Physics and Information Technology, Jining University, Qufu 273155, China*

(Received 31 July 2013; published 25 November 2013)

In this paper, we analyze the multiwavelength thermal ghost imaging with the spatial light modulating system (SLMS) and rotating ground glass plate (RGGP), respectively. We find that the multiwavelength ghost imaging dramatically enhances the signal-to-noise ratio (SNR) of ghost imaging for all types of objects. The N-wavelength ghost imaging with SLMS produces N^2 ghost images incoherently added together to form one ghost image whose SNR is N^2 times the one of single-wavelength ghost imaging. The N-wavelength ghost imaging with RGGP produces N ghost images incoherently added together to form one ghost image whose SNR is N times the one of single-wavelength ghost imaging. We find that a quantum effect is involved in the thermal light, although in a specific scenario at present. Moreover, the color ghost image obtained by the multiwavelength ghost imaging is better than the monochromatic ghost image in our observation.

DOI: 10.1103/PhysRevA.88.053842 PACS number(s): 42.50.−p, 42.30.Va

I. INTRODUCTION

Ghost imaging is a transverse imaging modality that exploits the cross correlation between two photocurrents, arising from the detection of two distinct but highly correlated optical beams. It is called ghost imaging because the photons that provide the spatial information regarding the object have never directly interacted with the object to be imaged.

The two light fields used in ghost imaging need not have the same wavelength [1–4]. Nondegenerate-wavelength quantum ghost imaging has already been demonstrated experimentally [2,4], although most thermal ghost imaging experiments have been carried out for the single-wavelength situation. Moreover, we can only obtain a monochromatic ghost image by the single-wavelength ghost imaging (SGI). However, the color ghost image obtained by ghost imaging with a multiwavelength source is better than the monochromatic ghost image in observation.

An important feature of ghost imaging is its significant application value [5–9]. How to enhance the image quality to match the classical optical imaging has become the focus of the study. The signal-to-noise ratio (SNR) shows how well the image of the object is distinguishable from the contrast and the resolution. Previous works [9–13] have investigated the method of calculating the SNR of ghost imaging with thermal and quantum sources. Especially, Ref. [14] has presented a technique called differential ghost imaging that dramatically enhances the SNR of ghost imaging. Most important, this method has been applied [15]. The SNR of differential ghost imaging becomes highly efficient when the object is a highly transparent object, but if the object is a highly absorbing object, the SNR of differential ghost imaging and conventional ghost imaging are quite similar.

In view of this, we present theoretically the multiwavelength ghost imaging with a spatial light modulating system (SLMS) and a rotating ground glass plate (RGGP), respectively. We find that the multiwavelength ghost imaging dramatically enhances the SNR of ghost imaging for all types of objects. At the same time, we first propose the concepts of autochannel and cross channel in ghost imaging. For simplicity, we shall utilize two quasimonochromatic light beams (red and green) to expound our work.

II. GHOST IMAGING WITH SPATIAL LIGHT MODULATING SYSTEM

In order to study the properties of multiwavelength ghost imaging, we consider the setup depicted in Fig. 1 (with SLMS). For thermal ghost imaging, two laser beams pass through the SLMS and then generate two light beams by a 50:50 beam splitter. In nondegenerate-wavelength thermal ghost imaging, the spatial correlations between the two beams can be produced by the amplitude mask that generates random spatial patterns following Gaussian statistics. Thus, two light fields are rendered spatially incoherent but in a correlated fashion [1].

In the ghost imaging setup, the two light beams are the signal, which interacts with the object $[T(\rho)]$ and then is measured by a bucket detector, and the reference, which is directly measured by a charge-coupled device (CCD) camera. The ghost imaging comes from the average intensities of light received by the bucket detector and the CCD camera, from the intensity cross-correlation function. Suppose that the photodetector response time is short compared with the correlation time of the optical field [16–18]. So we have

$$\hat{C}(\boldsymbol{\rho}_1) = \frac{1}{T_I}\int_{-T_I/2}^{T_I/2} dt\, \hat{\imath}_r(t)\hat{\imath}_s(t), \tag{1}$$

where [9, 19,20]

$$\hat{\imath}_m(t) = q\int du \int_{A_m} d\rho[\hat{E}^{\dagger}_{m1}(\rho,u)\hat{E}_{m1}(\rho,u) + \hat{E}^{\dagger}_{m2}(\boldsymbol{\rho},u)\hat{E}_{m2}(\boldsymbol{\rho},u)]h_B(t-u), \tag{2}$$

are the photocurrents produced by the two detectors, for $m = r,s$, with q being the electron charge, A_m being the

*yjxia@mail.qfnu.edu.cn

photosensitive region of bucket detector and CCD camera, T_I being the duration of the averaging interval, and $h_B(t)$ being the finite electrical bandwidth of the detectors.

The signal and reference beams are generated by the beam splitter. The field operators appearing in these photocurrent operators are

$$\hat{E}_{ml}(\rho,t) \equiv \begin{cases} [\sqrt{\eta}\,\hat{E}_l(\boldsymbol{\rho},t) + \sqrt{1-\eta}\,\hat{E}_{\mathrm{vac},l}(\boldsymbol{\rho},t)]h_{ml}(\rho), m = r; \\ [\sqrt{\eta}\,T(\boldsymbol{\rho})\,\hat{E}_l(\boldsymbol{\rho},t) + \sqrt{1-\eta|T(\boldsymbol{\rho})|^2}\,\hat{E}_{\mathrm{vac},l}(\boldsymbol{\rho},t)]h_{ml}(\rho), m = s, \end{cases} \tag{3}$$

where $m,l = (s,r),(1,2),\{\hat{E}_{\mathrm{vac},l}(\boldsymbol{\rho},t)\}$ are the vacuum states. η is the quantum efficiency of the detectors. The function $h_{ml}(\rho)$ is the Huygens-Fresnel Green's function that describe propagation through the object and reference arms,

$$h_{ml}(\rho) = \frac{k_l e^{ik_l(L+|\rho|^2/2L)}}{i2\pi L}, \tag{4}$$

$k_l = \omega_l/c$ is the wave number associated with the frequency. The $\hat{C}(\boldsymbol{\rho}_1)$ measurement yields an unbiased ensemble-average equal-time photocurrent cross-correlation function,

$$\begin{aligned}\langle \hat{C}(\rho_1)\rangle = \langle \hat{\imath}_1(t)\hat{\imath}_2(t)\rangle = q^2 A_s \int_{A_r} d\boldsymbol{\rho} \int du_1 \int du_2\, h_B(t-u_1)h_B(t-u_2)(\langle \hat{E}^\dagger_{r1}(\boldsymbol{\rho}_1,u_1)\hat{E}_{r1}(\boldsymbol{\rho}_1,u_1)\hat{E}^\dagger_{s1}(\boldsymbol{\rho},u_2)\hat{E}_{s1}(\boldsymbol{\rho},u_2)\rangle \\ + \langle \hat{E}^\dagger_{r2}(\boldsymbol{\rho}_1,u_1)\hat{E}_{r2}(\boldsymbol{\rho}_1,u_1)\hat{E}^\dagger_{s2}(\boldsymbol{\rho},u_2)\hat{E}_{s2}(\boldsymbol{\rho},u_2)\rangle + \langle \hat{E}^\dagger_{r1}(\boldsymbol{\rho}_1,u_1)\hat{E}_{r1}(\boldsymbol{\rho}_1,u_1)\hat{E}^\dagger_{s2}(\boldsymbol{\rho},u_2)\hat{E}_{s2}(\boldsymbol{\rho},u_2)\rangle \\ + \langle \hat{E}^\dagger_{r2}(\boldsymbol{\rho}_1,u_1)\hat{E}_{r2}(\boldsymbol{\rho}_1,u_1)\hat{E}^\dagger_{s1}(\boldsymbol{\rho},u_2)\hat{E}_{s1}(\boldsymbol{\rho},u_2)\rangle). \end{aligned} \tag{5}$$

The signal and reference field operators obey the canonical commutation relations [9–11,21,22]

$$\begin{aligned}&[\hat{E}_m(\boldsymbol{\rho}_1,t_1),\hat{E}_\ell(\boldsymbol{\rho}_2,t_2)] = 0; \\ &[\hat{E}_m(\boldsymbol{\rho}_1,t_1),\hat{E}^\dagger_\ell(\boldsymbol{\rho}_2,t_2)] = \delta_{m,\ell}\,\delta(\boldsymbol{\rho}_1-\boldsymbol{\rho}_2)\delta(t_1-t_2), \end{aligned} \tag{6}$$

for $m,\ell = s,r$. The four fourth-order moments can be expressed in terms of second-order moments by moment-factoring theorem for Gaussian-state optical fields [9–11,21]. Since this procedure is straightforward but tedious, we shall confine our discussion here to a detailed description of the simplification procedure, rather than a lengthy derivation.

First, we use the commutator relations (6) to put the integrand into normal order. Then, the Gaussian-state moment-factoring theorem is applied to each term, replacing higher-order moments with expressions that depend only on the second-order moments of the fields. Finally, we subtract the zero terms and the background terms [9,10,23–25]. Thus, we obtain the background-free ghost image,

$$\begin{aligned}\langle \hat{C}(\rho_1)\rangle = q^2 A_s \int_{A_r} d\boldsymbol{\rho} \int du_1 \int du_2\, h_B(t-u_1)h_B(t-u_2) \\ \times(|\langle \hat{E}^\dagger_{r1}(\boldsymbol{\rho}_1,u_1)\hat{E}_{s1}(\boldsymbol{\rho},u_2)\rangle|^2 \\ +|\langle \hat{E}^\dagger_{r2}(\boldsymbol{\rho}_1,u_1)\hat{E}_{s2}(\boldsymbol{\rho},u_2)\rangle|^2 \\ +|\langle \hat{E}^\dagger_{r1}(\boldsymbol{\rho}_1,u_1)\hat{E}_{s2}(\boldsymbol{\rho},u_2)\rangle|^2 \\ +|\langle \hat{E}^\dagger_{r2}(\boldsymbol{\rho}_1,u_1)\hat{E}_{s1}(\boldsymbol{\rho},u_2)\rangle|^2). \end{aligned} \tag{7}$$

For thermal source, the phase-insensitive cross correlation has maximum value, which is given by [9–11,21]

$$\begin{aligned}&\langle \hat{E}^\dagger_{sl}(\rho_1,t_1)\hat{E}_{rl}(\rho_2,t_2)\rangle \\ &= \eta|T(\rho)|\left(\frac{2P}{\pi a_0^2}\right)e^{-(|\boldsymbol{\rho}_1|^2+|\boldsymbol{\rho}_2|^2)/a_0^2-|\boldsymbol{\rho}_2-\boldsymbol{\rho}_1|^2/2\rho_0^2}, \end{aligned} \tag{8}$$

where $P = \int_{R^2} d\rho \langle \hat{E}^\dagger_m(\boldsymbol{\rho},t)\hat{E}_\ell(\boldsymbol{\rho},t)\rangle$ is the photon flux [9–11], a_0 is the e^{-2} attenuation radius of the transverse intensity profile, and ρ_0 is the transverse coherence radius. Substituting Eq. (8) into Eq. (7), we obtain the multiwavelength ghost image with SLMS,

$$\begin{aligned}\langle \hat{C}(\rho_1)\rangle &= q^2\eta^2 A_s\left(\frac{2}{\pi a_0^2}\right)^2 \\ &\times \int_{A_r} d\rho |T(\rho)|^2 e^{-2(|\boldsymbol{\rho}_1|^2+|\boldsymbol{\rho}_2|^2)/a_0^2-|\boldsymbol{\rho}_2-\boldsymbol{\rho}_1|^2/\rho_0^2} \\ &\times \left(P_r^2+P_g^2+P_b^2+P_b^2\right) \\ &= \langle \hat{C}_r(\rho_1)\rangle + \langle \hat{C}_g(\rho_1)\rangle + \langle \hat{C}_b(\rho_1)\rangle + \langle \hat{C}_b(\rho_1)\rangle, \end{aligned} \tag{9}$$

where r,g,b represent red, green, and blue, respectively.

Equation (9) shows that the two-wavelength ghost imaging with SLMS produces four ghost images (i.e., one red ghost image, one green ghost image, and two blue ghost images). Each ghost image is the same as the ghost image achieved by the single-wavelength ghost imaging [11,21]. The second-order thermal ghost imaging with two-wavelength yields four ghost images, whose nature is the correlations of degenerate-wavelength and nondegenerate-wavelength. Furthermore, we investigated the N-wavelength ghost imaging with SLMS, and found that the N^2 ghost images could be obtained.

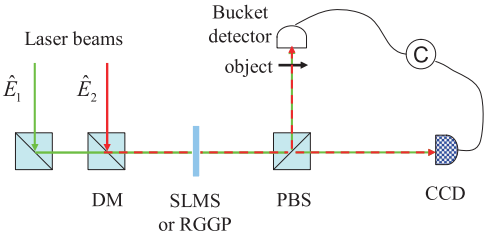

FIG. 1. (Color online) Setup for multiwavelength thermal ghost imaging with SLMS or RGGP. DM: dichroic mirror; PBS: polarizing beam splitter.

It is noted that the two-wavelength ghost imaging with SLMS not only produces the red and green ghost images, but also produces two blue ghost images. The two blue ghost images come from the cross correlations between $\hat{E}_{r1}$ and $\hat{E}_{s2}$, $\hat{E}_{r2}$, and $\hat{E}_{s1}$ (i.e., nondegenerate-wavelength correlations), while the red and green ghost images come from the cross correlations between the $\hat{E}_{r1}$ and $\hat{E}_{s1}$, $\hat{E}_{r2}$ and $\hat{E}_{s2}$ (i.e., degenerate-wavelength correlations). Since the red, green, and blue are the three primary colors, according to the color additive law [26], the red, green, and blue ghost images are incoherently added together to form one color ghost image.

For simplicity, we assume that the photon flux P are all the same for different wavelengths. When the intensity radius a_0 is much larger than the object's transverse extent, the entire object is uniformly illuminated on average. Moreover, to simplify our results, we shall assume that ρ_0 is sufficiently small to resolve all features in $T(\rho)$. Thus, we reduce Eq. (9) to

$$\langle \hat{C}(\rho_1)\rangle = q^2\eta^2 A_s A_r \left(\frac{2}{\pi a_0^2}\right)^2 \pi\rho_0^2 |T(\rho)|^2 (4P^2). \quad (10)$$

We will use the method that is given by Erkmen *et al.* [9–11] to obtain the signal-to-noise ratio of multiwavelength ghost imaging. The ghost image's SNR is defined as

$$\mathrm{SNR} \equiv \frac{\langle \hat{C}(\boldsymbol{\rho}_1)\rangle^2}{\langle \Delta\hat{C}^2(\boldsymbol{\rho}_1)\rangle}, \quad (11)$$

where $\Delta\hat{C}(\boldsymbol{\rho}) \equiv \hat{C}(\boldsymbol{\rho}) - \langle \hat{C}(\boldsymbol{\rho})\rangle$, i.e., it is the ratio of the squared strength of the ghost image component of the photocurrent cross correlation divided by the variance of that cross correlation. Following the method, we obtain the SNR's expression of the two-wavelength ghost imaging with SLMS,

$$\begin{aligned}\mathrm{SNR} &= \frac{4|T(\rho)|^4 T_I/T_0}{\frac{A_T'}{\sqrt{2\pi}\rho_0^2} + \frac{|T(\rho)|^2}{\eta\mathcal{I}} + \frac{4\pi\rho_0^2|T(\rho)|^4}{3A_s\eta\mathcal{I}} + \frac{\sqrt{\pi}\Omega_B T_0\rho_0^2|T(\rho)|^2}{16\sqrt{2}A_s\eta^2\mathcal{I}^2}} \\ &= 4(\mathrm{SNR}_{SGI}), \end{aligned} \quad (12)$$

where $\mathcal{I} = PT_0\rho_0^2/a_0^2$ is the brightness of source, Ω_B is the baseband bandwidth of the detector, T_0 is the coherence time, and $A_T' = \int d\rho |T(\rho)|^4$.

It is surprising that the SNR of two-wavelength ghost imaging with SLMS is four times the SNR of single-wavelength ghost imaging [10,11]. We also analyzed the SNR of N-wavelength ghost imaging with SLMS, and found that the SNR of N-wavelength ghost imaging with SLMS is N^2 times the one of the single-wavelength ghost imaging, which is very useful in application. This method is effective for all types of objects including the highly transparent and highly absorbing objects, as the ratio between the SNR of multiwavelength ghost imaging and single-wavelength ghost imaging is a constant that is independent of the object.

III. GHOST IMAGING WITH ROTATING GROUND GLASS PLATE

Let us consider in detail the analysis of multiwavelength ghost imaging with RGGP. In degenerate-wavelength thermal ghost imaging, typically a rotating ground glass plate is used to create two correlated copies of the spatially incoherent light beams. However, for nondegenerate-wavelength light fields, this method is not suitable for creating spatial correlations between the two fields [1]. The field operators appearing in the photocurrent operators are the same as those in Eq. (2). Substituting Eq. (2) into Eq. (1), we obtain

$$\begin{aligned}\langle \hat{C}(\rho_1)\rangle &= \langle \hat{\imath}_1(t)\hat{\imath}_2(t)\rangle \\ &= q^2 A_s \int_{A_r} d\boldsymbol{\rho} \int du_1 \int du_2\, h_B(t-u_1)h_B(t-u_2) \\ &\quad \times (\langle \hat{E}_{r1}^\dagger(\boldsymbol{\rho}_1,u_1)\hat{E}_{r1}(\boldsymbol{\rho}_1,u_1)\hat{E}_{s1}^\dagger(\boldsymbol{\rho},u_2)\hat{E}_{s1}(\boldsymbol{\rho},u_2)\rangle \\ &\quad + \langle \hat{E}_{r2}^\dagger(\boldsymbol{\rho}_1,u_1)\hat{E}_{r2}(\boldsymbol{\rho}_1,u_1)\hat{E}_{s2}^\dagger(\boldsymbol{\rho},u_2)\hat{E}_{s2}(\boldsymbol{\rho},u_2)\rangle). \end{aligned} \quad (13)$$

Here there is no cross correlation between the nondegenerate-wavelength light fields. Based on the above analysis, we obtain the two-wavelength ghost image with RGGP,

$$\begin{aligned}\langle \hat{C}(\rho_1)\rangle &= q^2\eta^2 A_s \left(\frac{2}{\pi a_0^2}\right)^2 \int_{A_r} d\rho\, |T(\rho)|^2 \\ &\quad \times e^{-2(|\boldsymbol{\rho}_1|^2+|\boldsymbol{\rho}_2|^2)/a_0^2 - |\boldsymbol{\rho}_2-\boldsymbol{\rho}_1|^2/\rho_0^2}\left(P_r^2 + P_g^2\right). \end{aligned} \quad (14)$$

Equation (14) shows that two ghost images (one red ghost image, and one green ghost image) are obtained by the two-wavelength ghost imaging with RGGP, which is similar to the red and green ghost images obtained by the two-wavelength ghost imaging with SLMS (i.e., degenerate-wavelength correlation). When the ghost imaging is achieved by the three-wavelength (red, green, and blue), we can also obtain the color ghost image, which effectively solves the problem that the monochromatic ghost image is not conducive to observation.

We obtain the SNR of two-wavelength ghost imaging with RGGP by the same method,

$$\begin{aligned}\mathrm{SNR} &= \frac{2|T(\rho)|^4 T_I/T_0}{\frac{A_T'}{\sqrt{2\pi}\rho_0^2} + \frac{|T(\rho)|^2}{\eta\mathcal{I}} + \frac{4\pi\rho_0^2|T(\rho)|^4}{3A_s\eta\mathcal{I}} + \frac{\sqrt{\pi}\Omega_B T_0\rho_0^2|T(\rho)|^2}{16\sqrt{2}A_s\eta^2\mathcal{I}^2}} \\ &= 2(\mathrm{SNR}_{SGI}). \end{aligned} \quad (15)$$

We also found that the SNR of N-wavelength ghost imaging with RGGP is N times the one of the single-wavelength ghost imaging.

IV. MULTICHANNEL ENHANCMENT OF SIGNAL-TO-NOISE RATIO

The inhibition of noise of multiwavelength ghost imaging with SLMS and RGGP can be explained by the extra channel of communication theory. We assume that one signal (ghost image) is transmitted by N information channels. Thus, the output signal of the ith channel can be expressed as

$$a_i = s + n_i, \quad (16)$$

where n_i is the noise of the Nth channel. Generally, the noise of each channel is different. s is the signal that is the same for all channels. Therefore, we obtain the total output signal

$$\Lambda = E\left\{\left(\sum_{i=1}^{N} a_i\right)^2\right\}, \quad (17)$$

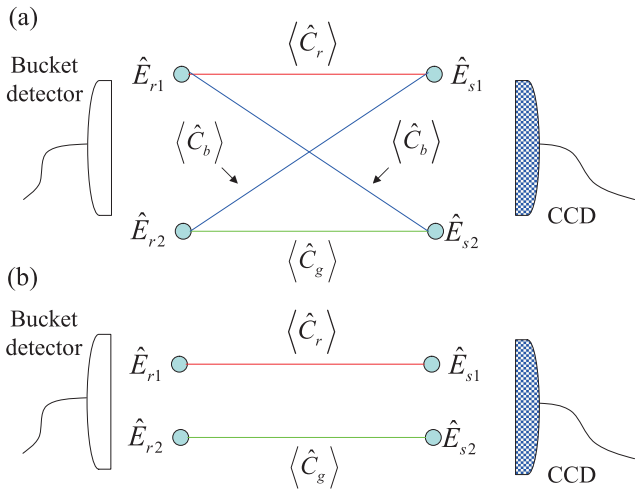

FIG. 2. (Color online) (a) The channels of multiwavelength ghost imaging with SLMS. Since the SLMS allows the light fields to have degenerate-wavelength and nondegenerate-wavelength correlations, the N-wavelength ghost imaging with SLMS has N^2 channels. (b) The channels of multiwavelength ghost imaging with RGGP. The RGGP makes the multiwavelength ghost imaging have only degenerate-wavelength correlation, but has no nondegenerate-wavelength correlation, so the N-wavelength ghost imaging with RGGP has N channels.

where $E\{\ldots\}$ represents the average. Substituting Eq. (16) into Eq. (17), we obtain

$$\Lambda = N^2 s^2 + 2Ns \sum_{i=1}^{N} E\{n_i\} + \sum_{i,j=1}^{N} E\{n_i n_j\}. \tag{18}$$

Since the noise is completely random, $E\{n_i\} = 0$. Moreover, the different noise uncorrelated, i.e.,

$$E\{n_i n_j\} = \begin{cases} 0, & i \neq j; \\ \sigma^2, & i = j, \end{cases} \tag{19}$$

where σ is the noise variance. The total output signal can be rewritten as

$$\Lambda = N^2 s^2 + N\sigma^2. \tag{20}$$

Equation (20) shows that the SNR of the single channel is s^2/σ^2, while the SNR of N channels is Ns^2/σ^2. Thus, the SNR can be enhanced N times by N information channels.

The twowavelength ghost imaging with SLMS [Fig. 2(a)] has two autochannels obtained by the degenerate-wavelength correlation [i.e., $\langle \hat{C}_r \rangle$ and $\langle \hat{C}_g \rangle$] and two cross channels obtained by the nondegenerate-wavelength correlation [i.e., $\langle \hat{C}_b \rangle$], while the twowavelength ghost imaging with RGGP [Fig. 2(b)] has only two autochannels. So the SNR of the multiwavelength ghost imaging with SLMS is larger than the case of RGGP. The autochannel is similar to the classical channel. However, the cross channel is a pure quantum behavior. The cross channel is obtained by the nondegenerate-wavelength correlation that is similar to the biphoton obtained by the spontaneous parametric down conversion (SPDC) [1,4,27]. The cross channel enables the ghost imaging to have the power of obtaining the ghost image by the nondegenerate-wavelength source. There will be no cross channel without nondegenerate-wavelength correlation, which is different from the classical channel. Therefore, the cross channel does not show in the classical optical imaging.

Experimental demonstration of ghost imaging, reported in 1995 [4], utilized the orthogonally polarized signal and idler beams produced by type-II phase-matched spontaneous parametric down conversion(SPDC). Consequently, the ghost imaging was claimed to be a quantum effect because an entangled-state light source was employed in its generation. Then the ghost imaging with pseudothermal source [28] and pure thermal source [29] were successively reported. There soon appeared a very passionate debate about whether the nature of ghost imaging or two-photon correlation is a quantum or classical effect. The classical statistical interpretation has been widely accepted at present. However, our research work shows that the viewpoint of Shih *et al.* may be correct, i.e., the nature of ghost imaging or two-photon correlation is a quantum effect.

Probably, the channel theory can contribute to this debate. The cross channel obtained by the nondegenerate-wavelength correlation can be seen as a good evidence to illustrate the quantum nature of ghost imaging. Reviewing the development of ghost imaging, previous ghost imaging including the quantum ghost imaging [4], computational ghost imaging [18,30], and other imaging scheme [7,14] based on the conventional ghost imaging can be divided into two classifications: the ghost imaging obtained by the classical light source (except the two-color ghost imaging with thermal source [1]), which can be described by the autochannel, shows a more classical effect; on the contrary, the ghost imaging obtained by the quantum light source (include the two-color ghost imaging with thermal source), which can be described by the cross channel, shows a quantum effect. The cross channel can be obtained by the thermal source, which shows that the pure quantum effect really exists in the thermal light field, although in a specific scenario at present.

Liu *et al.* [31] studied the Nth-order coherence of thermal light and have shown that the Nth-order coherence or correlation is quantum effect. The result of this paper supports the quantum interpretation of coherence or correlation of thermal light. The two blue ghost images obtained by the cross channel correspond to the "one way" and "another way" to trigger the joint detection event when $\lambda_j \neq \lambda_k$ respectively. The red and green ghost images obtained by the autochannel correspond to the two ways to trigger the joint detection event when $\lambda_j = \lambda_k$ respectively. At the same time, the interpretation also supports the channel theory of this paper. Furthermore, Ragy *et al.* [32] show that the quantum correlations exist even in "classicallike" thermal light sources. Consequently, the viewpoint of Shih *et al.* may be correct.

V. CONCLUSION

In this paper, the multiwavelength thermal ghost imaging with spatial light modulating system and rotating ground glass plate have been investigated. Our research work shows that the multiwavelength ghost image dramatically enhances the SNR of ghost imaging, which is effective for all types

of objects. The N-wavelength ghost imaging with SLMS yields N^2 ghost images incoherently added together to form one ghost image whose SNR is N^2 times the one of the single-wavelength ghost imaging. The N-wavelength ghost imaging with RGGP yields N ghost images incoherently added together to form one ghost image whose SNR is N times the single-wavelength case. Since the multiwavelength ghost imaging has more channels than the single-wavelength ghost imaging, the SNR of multiwavelength ghost imaging is larger than that of single-wavelength ghost imaging. Moreover, the SLMS allows the nondegenerate-wavelength field correlations to exist. Thus, the cross channel of multiwavelength ghost imaging with SLMS further enhances the signal-to-noise ratio.

The cross channel that is different from the classical channel shows that the quantum effect is involved in the thermal light. Therefore, the nature of ghost imaging may be the quantum effect, which supports the viewpoint of Shih *et al*.

Fortunately, the color ghost image can be obtained by multiwavelength ghost imaging with SLMS and RGGP. These two methods effectively solve the problem that the monochromatic ghost image is not conducive to observation in practice. We believe that this work will improve the image quality of ghost imaging.

ACKNOWLEDGMENTS

The authors wish to thank K. W. C. Chan for helpful discussions. This work was supported by the National Natural Science Foundation of China Grants No. 11204156 and No. 61178012.

[1] K. W. C. Chan, M. N. O'Sullivan, and R. W. Boyd, Phys. Rev. A **79**, 033808 (2009).
[2] S. Karmakar and Y. Shih, Phys. Rev. A **81**, 033845 (2010).
[3] Q. Liu, K.-H. Luo, X.-H. Chen, and L.-A. Wu, Chin. Phys. B **19**, 094211 (2010).
[4] T. B. Pittman, Y. H. Shih, D. V. Strekalov, and A. V. Sergienko, Phys. Rev. A **52**, R3429 (1995).
[5] K. W. C. Chan, D. S. Simon, A. V. Sergienko, N. D. Hardy, and J. H. Shapiro, Phys. Rev. A **84**, 043807 (2011).
[6] N. D. Hardy amd J. H. Shapiro, Phys. Rev. A **87**, 023820 (2013).
[7] M.-F. Li, Y.-R. Zhang, K.-H. Luo, L.-A. Wu, and H. Fan, Phys. Rev. A **87**, 033813 (2013).
[8] J. Cheng, Opt. Express **17**, 7916 (2009).
[9] N. D. Hardy, *Analyzing and Improving Image Quality in Reflective Ghost Imaging*, S.M. thesis (Massachusetts Institute of Technology, 2011).
[10] B. I. Erkmen and J. H. Shapiro, Phys. Rev. A **79**, 023833 (2009).
[11] B. I. Erkmen and J. H. Shapiro, Adv. Opt. Photon. **2**, 405 (2010).
[12] M. N. O'Sullivan, K. W. C. Chan, and R. W. Boyd, Phys. Rev. A **82**, 053803 (2010).
[13] G. Brida, M. V. Chekhova, G. A. Fornaro, M. Genovese, and E. D. Lopaeva, Phys. Rev. A **83**, 063807 (2011).
[14] F. Ferri, D. Magatti, L. A. Lugiato, and A. Gatti, Phys. Rev. Lett. **104**, 253603 (2010).
[15] M. Bina, D. Magatti, M. Molteni, A. Gatti, L. A. Lugiato, and F. Ferri, Phys. Rev. Lett. **110**, 083901 (2013).
[16] B. E. A. Saleh and M. C. Teich, *Noise in Classical and Quantum Photon-correlation Imaging*, Advances in Information Optics and Photonics Vol. PM183 (SPIE, Bellingham, 2008), Chap. 21.
[17] K. W. C. Chan, M. N. O'Sullivan, and R. W. Boyd, Opt. Lett. **34**, 3343 (2009).
[18] J. H. Shapiro, Phys. Rev. A **78**, 061802(R) (2008).
[19] J. H. Shapiro, Proc. SPIE **5111**, 382 (2003).
[20] R. Loudon, *The Quantum Theory of Light*, 3rd ed. (Oxford University Press, New York, 2000), Chap. 6.
[21] H. P. Yuen and J. H. Shapiro, IEEE Trans. Inf. Theor. **24**, 657 (1978).
[22] B. I. Erkmen and J. H. Shapiro, Phys. Rev. A **77**, 043809 (2008).
[23] H. Chen, T. Peng, and Y. Shih, Phys. Rev. A **88**, 023808 (2013).
[24] G. Scarcelli, V. Berardi, and Y. Shih, Phys. Rev. Lett. **96**, 063602 (2006).
[25] L. Basano and P. Ottonello, Appl. Phys. Lett. **89**, 091109 (2006).
[26] F. W. Billmeyer and Max Saltzman, *Principles of Color Technology*, 2nd ed. (Wiley-Interscience, New York, 1981).
[27] Y. Shih, arXiv:0805.1166.
[28] R. S. Bennink, S. J. Bentley, and R. W. Boyd, Phys. Rev. Lett. **89**, 113601 (2002).
[29] D. Zhang, Y.-H. Zhai, L.-A. Wu, and X.-H. Chen, Opt. Lett **30**, 2354 (2005).
[30] Y. Bromberg, O. Katz, and Y. Sillberberg, Phys. Rev. A **79**, 053840 (2009).
[31] J. Liu and Y. Shih, Phys. Rev. A **79**, 023819 (2009).
[32] S. Ragy and G. Adesso, Sci. Rep. **2**, 651 (2012).